Interaction between Aromatic Amine Cations and Quadrupolar Ligands: Infrared Spectra of Aniline$^+$−$(N_2)_n$ (n = 1−5) Complexes

Nicola Solcà and Otto Dopfer*

Institut für Physikalische Chemie, Universität Basel, Klingelbergstrasse 80, CH-4056 Basel, Switzerland

Received: April 3, 2002; In Final Form: June 3, 2002

Infrared (IR) photodissociation spectra of mass-selected aniline$^+$−$(N_2)_n$ complexes with $n \leq 5$, produced in an electron impact (EI) cluster ion source, are presented in the range of the N−H stretch vibrations of the aniline cation (An^+). Analysis of the An^+−N_2 spectrum is consistent with a H-bound structure in which the N_2 ligand forms a nearly linear hydrogen bond to one proton of the NH_2 group of An^+. No other isomers are observed in the $n = 1$ spectrum, implying that H-bound An^+−N_2 corresponds to the global minimum of the dimer potential. This conclusion is supported by ab initio calculations at the UMP2/6-311G(2df,2pd) level, which predict H-bound An^+−N_2 (D_e = 1431 cm^{-1}) to be more stable than other local minima. Systematic vibrational frequency shifts in the spectra of the larger An^+−$(N_2)_n$ clusters provide information about the microsolvation process of An^+ in a quadrupolar solvent. The first two N_2 ligands fill a first subshell by solvating the protons of the amino group (H bonds), whereas further ligands bind to the aromatic ring of An^+ (π bonds). Analysis of the photofragmentation branching ratios yields approximate dissociation energies of the H and π bonds of D_0(H) ∼ 1100 ± 300 cm^{-1} and $D_0(\pi)$ ∼ 700 ± 200 cm^{-1}, respectively.

1. Introduction

The solvation of an ion by neutral solvent molecules is a fundamental process for many phenomena in physical, organic, and biological chemistry,[1−3] because ion−ligand interactions have a much larger strength and longer range than corresponding neutral−neutral interactions.[4] Hence, the investigation of structure and stability of ionic complexes of the type A^+−L_n is of fundamental interest to model the stepwise solvation of a cation A^+ by a variable number of neutral ligands. In general, the shape of the intermolecular potential energy surface (PES) of a cation cluster is rather different from that of the corresponding neutral complex, as the additional charge provides substantial additional electrostatic and inductive contributions to the PES. In the present study, the intermolecular interaction between the aniline cation (An^+) and molecular nitrogen is characterized by infrared (IR) photodissociation spectroscopy and quantum chemical calculations of An^+−$(N_2)_n$ with $n \leq 5$. The analysis of the IR spectra elucidate the initial microsolvation process of An^+ in molecular nitrogen. This cluster system may be considered as a prototype for solvation of a positively charged aromatic amine in a polarizable quadrupolar solvent. Such interactions are relevant for biophysical processes in which charged amines interact with a hydrophobic environment.[5]

Aniline is the simplest aromatic amine and offers several attractive ligand binding sites. Possible sites include the π-electron system of the aromatic ring (π bond), the N atom of the amino group (N bond), and the protons of the aromatic ring (H^C bond) and the amino group (H bond). Spectrosocpic studies show that the preferred binding site strongly depends on the type of ligand and the charge state of aniline. For example, the nonpolar spherical rare gas (Rg) atoms prefer π bonds in the ground electronic state (S_0) of neutral An−Rg dimers, because dispersion interactions between the Rg atoms and the polarizable π-electron system are optimal in this configuration.[6−10] On the other hand, IR spectra of An^+−Ar suggest that the H bond in the cation ground state (D_0) of An^+−Rg dimers is more stable that the π bond, mainly because of the additional induction forces.[11,12] As an example for a strongly dipolar ligand, H_2O forms a N bond to An in S_0,[13] whereas the An^+−H_2O cation has a H-bound global minimum in D_0.[14,15]

N_2 is a polarizable diatomic with a nonvanishing negative quadrupole moment. Information about the structure of neutral An−N_2 in the two lowest singlet states, S_0 and S_1, comes from resonance enhanced multiphoton ionization (REMPI), laser induced fluorescence (LIF), and IR spectroscopy (combined with REMPI).[16−20] All spectroscopic results are consistent with a π-bound equilibrium structure of An−N_2 in both S_0 and S_1, with the N_2 molecule aligned parallel to the ring plane.[20] The binding energy in S_1 of ∼500 cm^{-1} is 130 cm^{-1} larger than in S_0,[17] leading to a shorter intermolecular π bond (3.43 Å in S_0 and 3.32 Å in S_1).[20] The D_0 state of the An^+−N_2 cation was investigated by zero kinetic energy (ZEKE) photoelectron[19,21] and one-color two-photon (1+1) REMPI−IR spectroscopy.[18] The results obtained with both techniques are not conclusive concerning the most stable binding site in An^+−N_2. The vibrational structure observed in the ZEKE spectra, obtained by REMPI via the π-bound S_1 state of An−N_2, was interpreted in terms of a π-bound equilibrium geometry in D_0.[19] On the other hand, the significant complexation-induced red shifts of the N−H stretch vibrations observed in the IR spectra of An^+−N_2 (also produced via REMPI of neutral π-bound An−N_2) were interpreted in terms of a H-bound equilibrium structure in D_0.[18]

Prior to the present work, all spectroscopic studies of An^+−N_2 are based on REMPI of the neutral An−N_2 dimer.[18,19,21] Recently, it was demonstrated that REMPI techniques for the generation and spectroscopic characterization of the most stable isomer of an aromatic cluster cation (A^+−L) often suffer from the severe restrictions imposed by the Franck−Condon (FC) principle.[11,22,23] In a usual REMPI scheme, mainly the most

* To whom correspondence should be addressed. E-mail: otto.dopfer@unibas.ch. Fax: +41 (61) 267 3855. Phone: +41 (61) 267 3823.

10.1021/jp020900x CCC: $22.00
Published on Web 07/17/2002

stable neutral A−L isomer in S_0 is formed in a supersonic expansion and subsequently ionized by either one-color (1+1) or two-color (1+1′) REMPI via S_1 to generate A^+−L dimers in D_0. As the PES of the cation dimer is often rather different from the PES of the neutral dimer, the FC factors for the REMPI process are frequently only favorable for the population of local minima of the cation dimer. In this case, the most stable isomer of a given cation cluster escapes experimental observation because of vanishing FC factors, with the consequence that wrong conclusions regarding the structure, stability, and dissociation energy of the most stable A^+−L cluster cation may be drawn. For example, REMPI of An−Ar and phenol−Ar (Ph−Ar) exclusively leads to the production of the π-bound An^+−Ar[19,24−27] and Ph^+−Ar[28−31] isomers, although for both complexes the global minimum in D_0 corresponds to the H-bound structure.[11,23,32] A similar situation may apply also to the An−N_2 dimer. Indeed, in analogy to Ph^+−N_2 and An^+−Ar,[11,22,31,33] the H-bound dimer is expected to be the global minimum of An^+−N_2, and this structure implies a large geometry change compared to the π-bound global minimum of neutral An−N_2. Interestingly, the production of the isoelectronic H-bound Ph^+−N_2 by REMPI does not suffer from the FC restrictions, because H-bound Ph−N_2 is more stable than π-bound Ph−N_2 also in the neutral ground state.[31,33]

In the present study, the limitations arising from the FC principle are overcome by using an electron impact (EI) ion source (rather than REMPI) for the generation of A^+−L_n cluster ions. The main production pathway of A^+−L_n in this ion source is the initial generation of A^+ by EI of A, followed by three-body clustering reactions to produce A^+−L_n.[23] According to this production scheme, this ion source produces predominantly the most stable isomer of a given A^+−L_n cluster ion, independent of the structure of the most stable neutral species.[11,22,23,32,34] Thus, one major goal of this study is the IR spectroscopic characterization of the intermolecular interaction of the An^+−N_2 dimer generated in the EI source, in order to unambiguously identify the global minimum structure in the D_0 state of this cation. The EI−IR spectra recorded in this way are compared with previous REMPI−IR spectra to discuss the differences between the EI and REMPI production of An^+−N_2. In addition, EI−IR spectra of larger An^+−$(N_2)_n$ clusters with $n \leq 5$ are presented for the first time to elucidate important properties of the microsolvation of An^+ in molecular nitrogen, such as cluster geometries, site-specific ligand binding energies, and structure of the first solvation shell. As no quantum chemical calculations of An^+−$(N_2)_n$ have been reported so far, ab initio and density functional calculations are carried out for clusters with $n \leq 2$ to support the interpretation of the experimental results.

2. Experimental Section

EI−IR photodissociation spectra of mass-selected An^+−$(N_2)_n$ complexes ($n = 1-5$) are recorded in a tandem mass spectrometer described elsewhere.[35] Briefly, the ion source combines a pulsed supersonic expansion with EI ionization. A heated An sample ($T \approx 330$ K) is seeded in N_2 at a backing pressure of 3−6 bar and expanded through a pulsed nozzle into vacuum. Ions and weakly bound ionic complexes are produced by EI ionization of the An/N_2 gas mixture close to the nozzle orifice and subsequent ion−molecule and clustering reactions in the high-pressure region of the expansion. Figure 1 shows a typical mass spectrum of the EI cluster ion source under the present experimental conditions. It is similar to the one discussed in a previous study of Ph^+−$(N_2)_n$ complexes using a Ph/N_2 mixture,[23] with the main difference that signals originating from

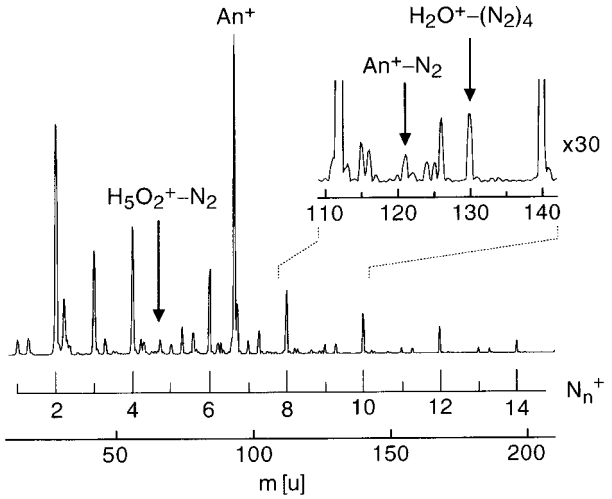

Figure 1. Mass spectrum of the electron impact cluster ion source for an expansion of heated An vapor seeded in N_2. The mass spectrum is dominated by N_n^+ (with strong even/odd alternation) and An^+. Only little fragmentation of An is observed upon EI ionization. Major cluster series include X^+−$(N_2)_n$, with X = N_2 and An, and several impurities, such as H_2O and H_5O_2.

Ph are replaced by those of An. As discussed in detail in ref 23, the major production mechanism of An^+−$(N_2)_n$ complexes is thought to begin with EI ionization of An followed by three-body association reactions according to

$$An + e^- \rightarrow An^+ + 2e^- \quad (1a)$$

$$An^+-(N_2)_{n-1} + N_2 + M \rightarrow An^+-(N_2)_n + M \quad \text{with } M = N_2 \text{ or An} \quad (1b)$$

This production scheme produces predominantly the most stable isomer of the An^+−$(N_2)_n$ cluster cations. All major peaks observed in the mass spectrum in Figure 1 can be assigned to An^+ and its fragment ions,[36] N_n^+, An^+−$(N_2)_n$, and contaminations of the type X^+−$(N_2)_n$ including $X^+ = H_2O^+$ and $H_5O_2^+$.

The central part of the expanding plasma is extracted through a skimmer into a quadrupole mass spectrometer, which is tuned to the mass of An^+−$(N_2)_n$. The mass selected parent beam is then injected into an octopole ion guide, where it is overlapped with a tunable IR laser pulse created by an optical parametric oscillator laser system with a bandwidth of 0.02 cm^{-1}. Resonant excitation into vibrational levels above the lowest dissociation threshold leads to fragmentation of An^+−$(N_2)_n$ according to the following laser-induced dissociation (LID) process:

$$An^+-(N_2)_n + \nu_{IR} \rightarrow An^+-(N_2)_n^* \rightarrow An^+-(N_2)_m + (n-m)N_2 \quad (2)$$

No other fragment channels are observed. Secondary sources of An^+−$(N_2)_m$ fragments originating from An^+−$(N_2)_n$ are collision-induced dissociation (CID) caused by residual gas and metastable decay (MD) of hot parent clusters in the octopole. The An^+−$(N_2)_m$ fragment ions are selected by a second quadrupole mass spectrometer and detected as a function of the IR frequency to obtain the EI−IR spectrum of An^+−$(N_2)_n$. To discriminate between LID and MD/CID signals, the ion source is triggered at twice the laser frequency (20 Hz), and the signals from alternating triggers are subtracted. The IR spectra are calibrated to better than 0.2 cm^{-1} by simultaneously recording optoacoustic spectra of ammonia.[37] For clusters with $n > 1$, several fragment channels m are possible, and IR action spectra

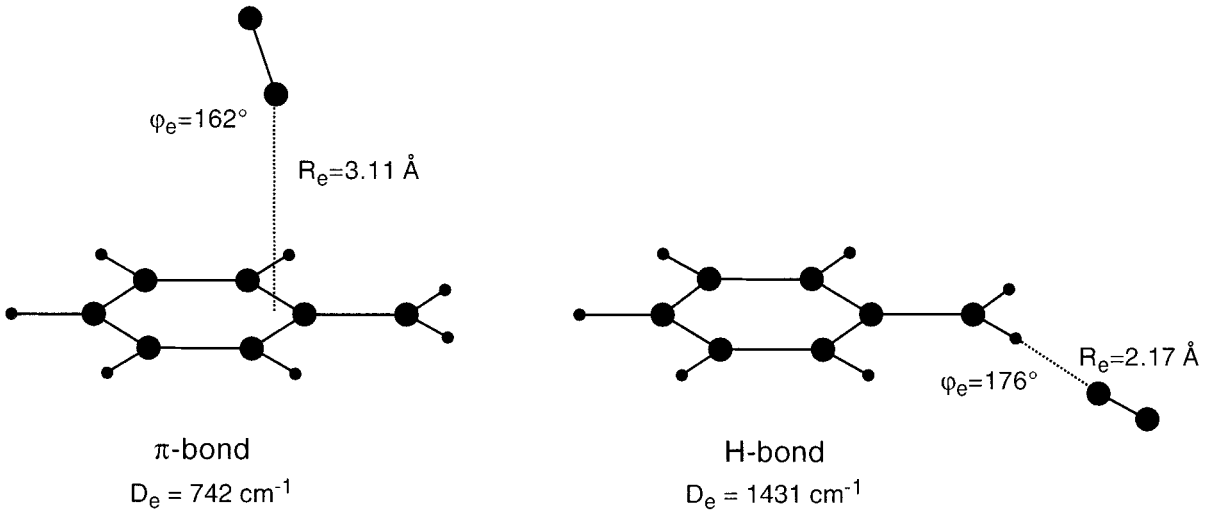

Figure 2. Equilibrium structures of the planar H-bound global minimum and the π-bound local minimum of An^+-N_2 calculated at the UMP2/6-311G(2df,2pd) level. Both geometries have C_s symmetry. Dissociation energies (D_e), intermolecular separations (R_e), and intermolecular bond angles (φ_e) are indicated.

TABLE 1: Selected Properties of $An^+-(N_2)_n$ ($n = 0-2$) Calculated at the B3LYP/6-31G* Level[a]

n	isomer	r_{NH} (Å)	ν_b [cm^{-1}]	ν_s [cm^{-1}]	ν_a [cm^{-1}]	D_e [cm^{-1}]
0		1.0156	1627.4 (116)	3388.1 (253)	3490.7 (89)	
1	H	1.0203/1.0157	1639.8 (103)	3342.9 (626)	3465.3 (155)	1174
1	π	1.0155/1.0155	1627.7 (114)	3389.1 (246)	3491.7 (87)	206
2	HH	1.0198/1.0198	1650.9 (89)	3328.1 (734)	3428.7 (388)	1105

[a] Harmonic frequencies are scaled by a factor of 0.95663. IR intensities in km/mol are listed in parentheses.

are taken simultaneously in the two dominant channels. All IR spectra are normalized for laser intensity variations measured with an InSb detector.

A complication arises from the fact that $An^+-(N_2)_n$ and $H_5O_2^+-(N_2)_p$ with $p = n + 2$ have the same mass and cannot be discriminated by the quadrupole mass spectrometers. The mass spectrum in Figure 1 indicates the significant abundance of both $H_5O_2^+$ ($m = 37$ u) and $H_5O_2^+-N_2$ ($m = 65$ u) in the ion source. Thus, the mass-selected $An^+-(N_2)_n$ ion beam is expected to be contaminated by $H_5O_2^+-(N_2)_p$ with $p = n + 2$. However, both cluster series can be distinguished by their different IR spectra and photofragmentation branching ratios (section 4.2).

3. Quantum Chemical Calculations

Ab initio and density functional calculations[38] are carried out for $An^+-(N_2)_n$ ($n = 0-2$) at the UMP2(fc)/6-311G(2df,2pd) and B3LYP/6-31G* levels of theory to investigate the intermolecular interaction between An^+ and N_2 as well as the effects of N_2 complexation on the properties of An^+. Previous calculations of isoelectronic Ph^+-N_2 demonstrate that the UMP2(fc)/6-311G(2df,2pd) level correctly reproduces the relative interaction energies of different binding sites.[22] Hence, this level is selected to evaluate the relative stability of various An^+-N_2 isomers. On the other hand, the lower B3LYP/6-31G* level is chosen to predict vibrational properties of $An^+-(N_2)_n$ ($n = 0-2$) relevant for the present study, such as harmonic frequencies and IR intensities. All coordinates are relaxed during the search for stationary points, and all interaction and dissociation energies are counter-poise corrected for basis set superposition error.[39]

The optimized geometries of π-bound and H-bound An^+-N_2 and their relevant structural parameters calculated at the UMP2/6-311G(2df,2pd) level are summarized in Figure 2. Similar to Ph^+-N_2,[22] the planar H-bound An^+-N_2 dimer corresponds to the global minimum of the PES ($D_e = 1431$ cm^{-1}), whereas the π-bound isomer is a significantly less stable local minimum ($D_e = 742$ cm^{-1}). The planar H-bound dimer features a slightly nonlinear proton bond ($\varphi_e = 176°$) with an intermolecular H−N separation of $R_e = 2.17$ Å. In the π-bound structure, the N_2 molecule is attached in a perpendicular fashion to the aromatic ring, interacting mainly with the ipso C atom at a separation of 3.11 Å between the ring plane and N_2. Although the interaction for π-bound An^+-N_2 is severely underestimated at the B3LYP/6-31G* level (Table 1), the structures of π/H-bound An^+-N_2 agree qualitatively with those calculated at the UMP2 level.

The vibrational properties of $An^+-(N_2)_n$ ($n = 0-2$) are evaluated at the B3LYP/6-31G* level, and the results relevant for the present work are collected in Table 1. The harmonic frequencies are scaled by a factor 0.95663 to optimize the agreement between the experimental[40] and calculated N−H stretch fundamentals of bare An^+. The resonant interaction between the two equivalent local N−H stretch modes of bare An^+ gives rise to the symmetric and antisymmetric N−H stretch normal modes, ν_s and ν_a. The resulting coupling is relatively strong and produces a calculated splitting of 103 cm^{-1} between ν_a and ν_s, which is close to the experimental value (93 cm^{-1}).[40] In H-bound An^+-N_2, the N−H bond adjacent to the intermolecular bond is significantly elongated compared to bare An^+ ($\Delta r_{NH} = 0.0047$ Å), whereas the free N−H bond is less affected upon complexation ($\Delta r_{NH} = 0.0001$ Å). Analysis of the ν_s and ν_a normal modes in H-bound An^+-N_2 indicates only partial decoupling into purely bound and free local N−H stretch modes. Consequently, both ν_s and ν_a feature significant contributions of the bound N−H stretch (75 and 25%). Thus, the frequencies of both modes are reduced upon N_2 complexation ($\Delta\nu_s = -45$ cm^{-1} and $\Delta\nu_a = -25$ cm^{-1}), and their intensities increase (by 147 and 74%). In addition to the N−H stretch fundamentals, the first overtone of the symmetric in-plane bend of the NH_2 group, denoted ν_b, is expected in the spectral range investi-

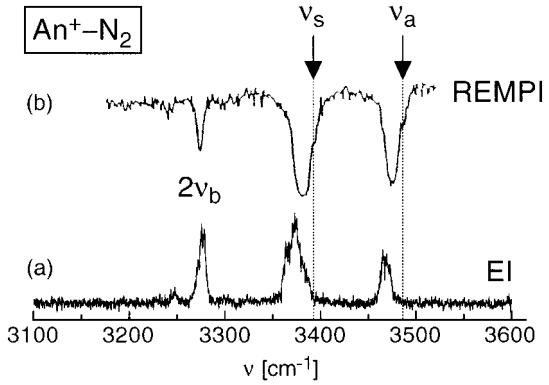

Figure 3. IR photodissociation spectra of An^+-N_2 in the range of the N−H stretch vibrations: (a) EI−IR spectrum; (b) REMPI−IR spectrum of An^+-N_2 generated by (1+1) REMPI of neutral $An-N_2$ (reproduced from ref 18). Arrows and dotted lines indicate the positions of the ν_s and ν_a fundamentals of bare An^+ at 3393 and 3486 cm^{-1} (ref 40).

gated.[11] The ν_b fundamental of bare An^+ is approximated as 1635 cm^{-1} by the experimental ν_b frequency of π-bound An^+-Ar and An^+ embedded in an Ar matrix,[26,41] in good agreement with the calculated value of An^+ (1627 cm^{-1}). The calculations predict a blue shift upon hydrogen bonding with N_2, $\Delta\nu_b = +12.4$ cm^{-1}, because of the additional retarding force arising from the intermolecular bond. Moreover, the IR intensity of ν_b decreases slightly. In contrast to H bonding, a π-bound N_2 ligand has little effect on the properties of the N−H bonds. Consequently, the calculated ν_s and ν_a frequencies of π-bound An^+-N_2 display only a ~1 cm^{-1} blue shift upon complexation and a negligible decrease in the IR intensities (Table 1). The fact that the B3LYP/6-31G* level severely underestimates the interaction for π bonding is not critical for comparison with the present experimental data because the effects of π bonding on the observed spectral features are small. For example, the experimental N−H stretch frequencies of An^+ and π-bound An^+-Ar agree to within 3 cm^{-1}.[11,12,27,40]

Both N−H stretch oscillators are again equivalent in the planar $An^+-(N_2)_2$ trimer in which both N_2 ligands form intermolecular proton bonds to the amino group of An^+ (HH isomer, C_{2v} symmetry). The N−H bonds of this structure are elongated by $\Delta r_{NH} = 0.0042$ Å compared to bare An^+. Accordingly, both ν_s and ν_a display similar total red shifts with respect to An^+ ($\Delta\nu_s = -60$ cm^{-1}, $\Delta\nu_a = -62$ cm^{-1}). Moreover, the IR intensities of ν_s and ν_a are enhanced by factors of ~3 and ~4, respectively. The H-bound ligands in the trimer maximize the retarding force for the bending motion of the NH_2 group, inducing a total blue shift of $\Delta\nu_b = +23.5$ cm^{-1}. The binding energy of the N_2 ligands in $An^+-(N_2)_2$ calculated at the B3LYP level ($D_e = 1105$ cm^{-1}) is somewhat smaller than in An^+-N_2 ($D_e = 1174$ cm^{-1}), implying that three-body forces of H-bound ligands are slightly noncooperative.

In summary, the calculations suggest that the H-bound dimer corresponds to the global minimum on the An^+-N_2 PES, whereas the π-bound isomer represents a local minimum (Figure 2). Both isomers can clearly be distinguished by their characteristic N−H stretch frequencies. According to the dimer potential, the cluster growth in $An^+-(N_2)_n$ begins by the solvation of the two protons of the amino group ($n = 1,2$) and proceeds by the attachment of further ligands to the aromatic ring ($n \geq 3$).

4. Experimental Results and Discussion

4.1. An^+-N_2 Dimer. Figure 3 compares the IR spectra of An^+-N_2 produced in the EI source (a) and by (1+1) REMPI (b, ref 18) in the range of the N−H stretch fundamentals. At least four bands are discernible in the EI−IR spectrum between 3100 and 3600 cm^{-1}, and their positions, widths, and assignments are listed in Table 2. The peaks at 3372 and 3468 cm^{-1} are unambiguously assigned to the ν_s and ν_a fundamentals of H-bound An^+-N_2, because of their significant red shifts ($\Delta\nu_s = -21$ and $\Delta\nu_a = -18$ cm^{-1}) compared to the corresponding vibrations of bare An^+ (indicated by arrows in Figure 3, $\nu_s = 3393$ cm^{-1}, $\nu_a = 3486$ cm^{-1}).[40] The corresponding shifts calculated at the B3LYP/6-31G* level are somewhat larger ($\Delta\nu_s = -45$ and $\Delta\nu_a = -25$ cm^{-1}). The same trend was also observed for the related H-bound An^+-Ar dimer.[11] Moreover, the small experimental difference, $|\Delta\nu_s - \Delta\nu_a| = 3$ cm^{-1}, suggests that the decoupling of the two local N−H stretch oscillators in H-bound An^+-N_2 is much weaker than predicted by the calculations ($|\Delta\nu_s - \Delta\nu_a| = 20$ cm^{-1}). However, both experimentally and theoretically, $|\Delta\nu_s|$ is larger than $|\Delta\nu_a|$, confirming that the ν_s normal mode carries a larger contribution of the bound N−H stretch. This observation is also consistent with the band contours observed in Figure 3a. The ν_s band at 3372 cm^{-1} shows a higher frequency tail, because the intermolecular bond becomes shorter upon vibrational excitation of a proton donor stretch, resulting in a blue shaded band contour with a band head in the P branch.[4,22,42−45] On the other hand, ν_a features a smaller contribution of the bound N−H stretch, and the intermolecular bond contraction upon ν_a excitation is less pronounced, resulting in a more symmetric band profile. The observed relative intensities of the two N−H stretching modes ($I_s/I_a \sim 2.6$) are also in qualitative agreement with the calculated ratio ($I_s/I_a \sim 4$).

In general, π-bound ligands in complexes of substituted aromatic molecules have little influence on the X−H stretch vibrations of the substituent and induce usually only a small blue shift compared to the corresponding monomer values. For example, the blue shifts are $\Delta\nu_{s/a} = 1-3$ cm^{-1} for π-bound An^+-Ar[11,27,40] and $\Delta\nu_1 = 1-2$ cm^{-1} for π-bound Ph^+-Ar/Kr.[23,28] Thus, the ν_s and ν_a fundamentals of π-bound An^+-N_2 are also expected to be only slightly blue shifted compared to An^+ (see arrows in Figure 3), in agreement with the predicted frequency shifts (Table 1). However, no signal is observed in this spectral range in the EI−IR spectrum of An^+-N_2, indicating that the abundance of π-bound An^+-N_2 is below the detection limit. As the EI source predominantly produces the most stable cation isomer, it is concluded that the global minimum on the PES of An^+-N_2 corresponds indeed to the H-bound structure, as predicted by the calculations (Figure 2). Probably, the large difference in the binding energies of both

TABLE 2: Band Maxima, Widths (fwhm, in Parentheses), and Shifts (All in cm^{-1}), along with Assignments of Vibrational Transitions Observed in the EI−IR Photodissociation Spectra of $An^+-(N_2)_n$ Recorded in the Dominant Fragment Channel (Figure 4)

n	position	shift[a]	assignment	*n*	position	shift[a]	assignment
1	3248 (6)			3	3359 (10)	−34	ν_s
1	3277 (10)	7	$2\nu_b$	3	3440 (8)	−46	ν_a
1	3372 (20)	−21	ν_s	4	3277 (6)	7	$2\nu_b$
1	3468 (12)	−18	ν_a	4	3360 (8)	−33	ν_s
2	3283 (7)	13	$2\nu_b$	4	3444 (6)	−42	ν_a
2	3366 (10)	−27	ν_s	5	3274 (6)	4	$2\nu_b$
2	3433 (14)	−53	ν_a	5	3362 (7)	−31	ν_s
3	3282 (8)	12	$2\nu_b$	5	3447 (9)	−39	ν_a

[a] Shifts of ν_s and ν_a are given with respect to the transitions of bare An^+ at $\nu_s = 3393$ cm^{-1} and $\nu_a = 3486$ cm^{-1} (ref 40). Shifts of $2\nu_b$ are given with respect to the transition of H-bound An^+-Ar at $2\nu_b = 3270$ cm^{-1} (ref 11).

isomers and/or a low isomerization barrier from the π-bound toward the H-bound structure are responsible for the low population of the π-bound isomer in the molecular beam. A similar situation was observed for isoelectronic Ph^+-N_2, where the H-bound dimer was clearly identified as the most stable isomer and no signature of the π-bound local minimum was observed in the EI−IR spectrum.[22,23] On the basis of the calculated relative IR intensities of the N−H stretch fundamentals of π-bound and H-bound An^+-N_2 (Table 1), the signal-to-noise ratio observed in Figure 3a (~10) provides an upper limit of ~25% for the relative abundance of the π-bound isomer in the expansion.

Besides the assigned N−H stretch modes, no other strong IR active fundamental of An^+-N_2 is predicted in the spectral range explored in Figure 3. Thus, the other two observed bands must be attributed to overtone or combination bands. The relatively intense peak at 3277 cm^{-1} is assigned to the first overtone of the symmetric in-plane bending mode of the NH_2 group, $2\nu_b$. This transition is also observed for the related An^+-Ar dimer at 3270 cm^{-1}.[11] The blue shift of the $2\nu_b$ overtone in H-bound An^+-N_2 is 7 cm^{-1} larger than for H-bound An^+-Ar,[11] because the additional retarding force upon hydrogen bonding is stronger for N_2 complexation due to the larger interaction. The weak transition at 3248 cm^{-1} appears also in the REMPI−IR spectra of other An^+-L clusters (e.g., L = N_2, CH_4, CHF_3, CO).[18] However, its interpretation is not clear, and further experiments are required to ascertain a definitive assignment.

Figure 3b reproduces the (1+1) REMPI−IR spectrum of An^+-N_2 reported in ref 18. This spectrum is similar in appearance to the EI−IR spectrum in Figure 3a. Similar to the EI−IR spectrum, the maxima of the ν_s and ν_a transitions in the REMPI−IR spectrum are clearly shifted to the red of the corresponding An^+ transitions. Moreover, the complexation-induced shifts, $\Delta\nu_s$ and $\Delta\nu_a$, observed in the REMPI−IR spectra of An^+-L (L = N_2, CO, CH_4) show a linear correlation to the proton affinities of the ligands L, indicating that these ligands form a H bond to the NH_2 group.[18] Consequently, the peaks observed in Figure 3b have tentatively been assigned to H-bound An^+-N_2.[18] As ionization in the REMPI−IR spectrum was accomplished via the S_1 origin of π-bound $An-N_2$,[18,20] an isomerization process from π-bound to H-bound An^+-N_2 was invoked to explain this observation.[18] Closer inspection of Figure 3 reveals that the maxima of ν_s and ν_a observed by in the REMPI−IR spectrum (3382 and 3476 cm^{-1}) are significantly shifted to higher frequencies (by 10 and 8 cm^{-1}) from the corresponding bands observed in the EI−IR spectrum (3372 and 3468 cm^{-1}). This discrepancy is attributed to different cluster temperatures in both IR spectra. The H-bound An^+-N_2 dimers produced in the EI ion source are vibrationally cold because of their formation in a three-body association reaction in a supersonic beam (eq 1b). In contrast, the H-bound An^+-N_2 dimers probed in the REMPI−IR spectrum are produced by (1+1) REMPI of π-bound $An-N_2$ with an excess energy of ~5000 cm^{-1} and subsequent isomerization. Hence, most of these H-bound An^+-N_2 dimers are expected to have significant excitation of intermolecular degrees of freedom. Accordingly, the transitions observed in the REMPI−IR spectra are probably not due to ν_s and ν_a fundamentals of H-bound An^+-N_2 but arise mainly from sequence transitions of the form $\nu_{s/a} + \nu_x \leftarrow \nu_x$, where ν_x are intermolecular vibrations. Such sequence transitions occur usually at a higher frequency than the corresponding fundamentals of proton donor stretch vibrations.[4,22,35,43,44] The $\nu_{s/a}$ bands in the REMPI−IR spectrum of An^+-N_2 display weaker unresolved shoulders close to the position of the $\nu_{s/a}$ fundamentals of bare An^+. These signals may arise from π-bound An^+-N_2 dimers which do not undergo isomerization to the more stable H-bound An^+-N_2 structure on the time scale of the experiment (the delay between the UV and IR lasers is 50 ns in ref 18).

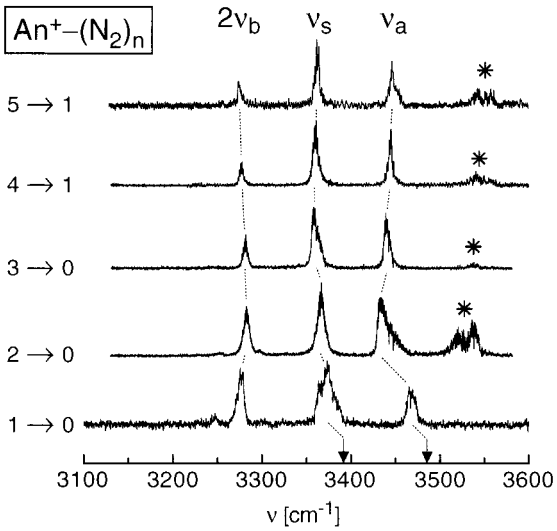

Figure 4. EI−IR photodissociation spectra of $An^+-(N_2)_n$ recorded in the dominant $An^+-(N_2)_m$ fragment channel (indicated as $n \rightarrow m$). The assignments to $An^+-(N_2)_n$ transitions are indicated. Peaks marked with asterisks originate from the contamination $H_5O_2^+-(N_2)_{n+2}$. The arrows on the wavenumber scale indicate the ν_s and ν_a fundamentals of bare An^+ at 3393 and 3486 cm^{-1} (ref 40).

4.2. Larger $An^+-(N_2)_n$ Clusters (n = 2−5). Figure 4 compares the EI−IR photodissociation spectra of $An^+-(N_2)_n$ (n = 1−5) in the vicinity of the N−H stretch vibrations of An^+. The transitions observed for An^+-N_2 show systematic shifts upon further N_2 complexation, providing useful information about the structure of the first solvation shell. The maxima, widths, and assignments of these transitions are listed in Table 2. Figure 5 visualizes the frequencies of ν_s, ν_a, their averaged value (ν_{av}), and $2\nu_b$ of $An^+-(N_2)_n$ as a function of the cluster size. The spectra of $An^+-(N_2)_n$ with $n \geq 2$ display additional transition(s) between 3515 and 3565 cm^{-1} (marked by asterisks in Figure 4). The carrier of these bands is identified as $H_5O_2^+-(N_2)_{n+2}$, which contaminates the $An^+-(N_2)_n$ mass channel (section 2).

As discussed in section 4.1, in the most stable An^+-N_2 dimer, the N_2 ligand forms a H bond to one proton of the NH_2 group of An^+. Thus, the second N_2 ligand is expected to solvate the second proton of the NH_2 group, leading to a planar $An^+-(N_2)_2$ trimer with two equivalent intermolecular H bonds (HH isomer, C_{2v} symmetry, Figure 6). The EI−IR spectrum of $An^+-(N_2)_2$ confirms this expectation. Similar to the dimer, attachment of the second ligand induces a noticeable red shift of ν_s and ν_a, because both modes contain a significant contribution of the free N−H oscillator in the H-bound dimer (section 3). The incremental complexation-induced shift, $\Delta\nu(n) = \nu(n) - \nu(n-1)$, is larger for ν_a than for ν_s, $\Delta\nu_a(2) = -35$ cm^{-1} and $\Delta\nu_s(2) = -6$ cm^{-1}, because ν_a features a larger contribution of the free N−H stretch. The corresponding calculated shifts are $\Delta\nu_a(2) = -37$ cm^{-1} and $\Delta\nu_s(2) = -15$ cm^{-1}, in qualitative agreement with the experiment. The total red shift is larger for ν_a than for ν_s (−53 vs −27 cm^{-1}), implying that the coupling between both N−H stretch local modes in $An^+-(N_2)_2$ is significantly smaller than in An^+: $\nu_a - \nu_s$ = 93 and 67 cm^{-1} for n = 0 and 2, respectively. In addition, excitation of ν_a has a stronger stabilizing effect on the intermolecular bonds than

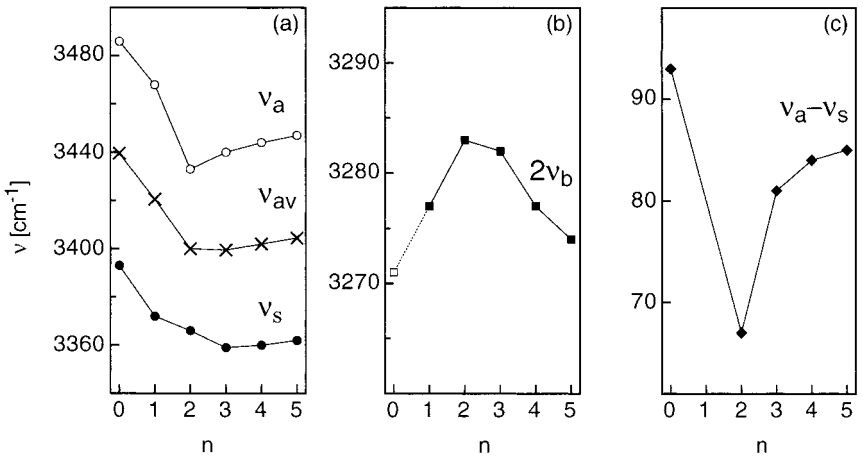

Figure 5. Plots of various vibrational frequencies of $An^+-(N_2)_n$ as a function of the cluster size (Table 2): (a) ν_a, ν_s, and their averaged value ν_{av}; (b) the $2\nu_b$ overtone; (c) the difference $\nu_a-\nu_s$. The open square in b corresponds to an extrapolation for $2\nu_b$ of bare An^+.

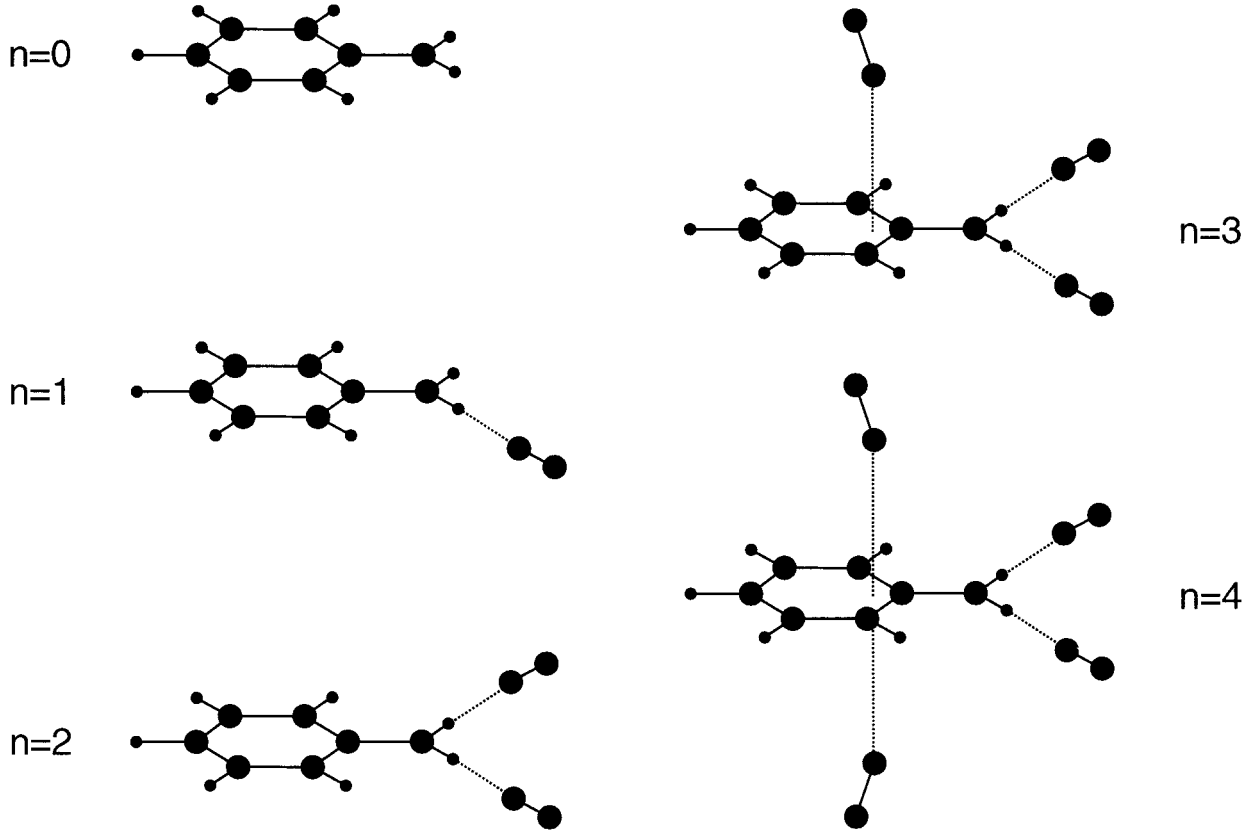

Figure 6. Sketch of the most stable cluster structures of $An^+-(N_2)_n$ with $n = 0$ (C_{2v}), 1 (C_s), 2 (C_{2v}), 3 (C_s), and 4 (C_{2v}), visualizing the sequential cluster growth deduced from the IR spectra.

excitation of ν_s. As a consequence, the formation of a P branch head is more pronounced for ν_a.

The average frequency of ν_s and ν_a, ν_{av}, is a measure of the N−H bond strength in $An^+-(N_2)_n$. The nearly additive interaction of the first two N_2 ligands with the amino group of An^+ results in an almost linear red shift of $\Delta\nu_{av} \sim -20$ cm^{-1} per N_2 ligand, indicating that three-body forces are small and noncooperative (Figure 5a). The corresponding calculated value amounts to ~-30 cm^{-1} per N_2 molecule. The first overtone of ν_b in $An^+-(N_2)_2$ is 6 cm^{-1} shifted to the blue compared to the dimer. Assuming additivity for $\Delta 2\nu_b$ upon sequential N_2 complexation, $2\nu_b$ of bare An^+ is estimated as 3271 cm^{-1}. This value approaches that of H-bound An^+-Ar (3270 cm^{-1}),[11] which closely approximates the frequency of bare An^+ (Figure 5b). The EI−IR spectrum of $An^+-(N_2)_2$ is dominated by the ν_s, ν_a, and $2\nu_b$ transitions of the most stable trimer (i.e., the HH isomer) and does not show any convincing evidence for the presence of less stable clusters, such as the Hπ and $\pi\pi$ isomers. This observation provides further evidence that the proton bonds in $An^+-(N_2)_n$ are more stable than the π bonds. For completeness, it is noted that the $An^+-(N_2)_2$ spectrum features two very weak but clearly reproducible transitions at 3253 and 3297 cm^{-1}. The first one probably correlates with the 3248 cm^{-1} band of An^+-N_2.

Both NH_2 protons are solvated in $An^+-(N_2)_2$, implying the closure of the first subshell within the first solvation shell (Figure 6). As the An^+-N_2 interaction is much stronger than the N_2-N_2 interaction ($D_e < 10^2$ cm^{-1}), further ligands are expected

to fill a solvation shell around an interior An^+ cation. For example, N_2 ligands can form a π bond to the ipso C atom (Figure 2). Alternative binding sites include binding to one or two neighboring H atoms of the aromatic ring (linear or bridged H^C bonds). Both π bonding and H^C bonding can be rationalzed by considering the analysis of the charge distribution in An^+,[11] which features significant positive atomic charges on the ipso C atom (+0.60 e) and each ring H atom (+0.12 e). The large charge on the ipso C atom favors π bonding over other ring binding sites due to the stronger electrostatic and inductive interaction with the quadrupolar, polarizable N_2 ligands. Moreover, dispersion interactions between N_2 and the π-electron system of the aromatic ring also favor π-bound geometries. Hence, the third and fourth N_2 ligand are expected to form π bonds as shown in Figure 6, and the analysis of the IR spectra of $An^+-(N_2)_3$ and $An^+-(N_2)_4$ described below confirm this prediction.

The average N−H bond length decreases slightly upon further solvation of $An^+-(N_2)_2$, manifesting itself as a small averaged increase in $\Delta\nu_{av}(n)$ of ~1.5 cm^{-1} per N_2 ligand ($n = 3-5$, Figure 5a). At the same time, the intermolecular proton bonds become weaker and the frequency of $2\nu_b$ decreases accordingly. The evolution of $\Delta\nu_{av}(n)$ and $\Delta 2\nu_b(n)$ for $n \geq 3$ does not provide conclusive information to clearly distinguish between π bonding and other ring binding sites. However, the coupling of the N−H stretch modes of the amino group appears to be very sensitive to the degree of solvation (Figure 5c) and may contain more specific information about the sequence of the solvation process. For An^+ and $An^+-(N_2)_n$ with $n \geq 2$, the magnitude of the splitting $\nu_a-\nu_s$ is a direct measure of the coupling between the two (solvated) local N−H oscillators of the amino group. H bonding strongly reduces this splitting from 93 ($n = 0$) to 67 cm^{-1} ($n = 2$), probably due to the destabilization of the N−H bonds (Figure 5c). The force constants of the (solvated) N−H bonds are not changing much upon further solvation, as demonstrated by the little increase of $\Delta\nu_{av}(n)$ for $n \geq 3$. Thus, the large observed increase in $\nu_a - \nu_s$ from $n = 2$ (67 cm^{-1}) to $n = 3$ (81 cm^{-1}) indicates a noticeable structural change of the (solvated) N−H bonds. As H^C bonds are unlikely to induce such an effect, this observation is taken as strong evidence that the third N_2 ligand forms indeed a π bond to the ipso C atom (Figure 6), implying C_s symmetry for the $An^+-(N_2)_3$ structure. The fourth ligand probably forms also a π bond but on the opposite side of the aromatic plane (Figure 6), leading to C_{2v} symmetry for $An^+-(N_2)_4$. The much smaller increase in $\nu_a - \nu_s$ from $n = 3$ (81 cm^{-1}) to $n = 4$ (84 cm^{-1}) suggests that the equivalent π bonds in $An^+-(N_2)_4$ are significantly weaker than the π bond in $An^+-(N_2)_3$. Such noncooperative three-body forces have previously been observed and calculated for similar p bonds in related ionic complexes, such as $CH_3^+-Ar_n$,[46] $H_2O^+-Ar_n$,[42,47] and $NH_3^+-Ar_n$.[45,48] The binding sites of the fifth and further ligands are not obvious. The coupling of the two N−H oscillators in $An^+-(N_2)_5$ ($\nu_a - \nu_s = 85$ cm^{-1}) is very similar to $An^+-(N_2)_4$, indicating that further changes in the geometry of the (solvated) amino group are very small. This observation is compatible with binding sites for the fifth ligand far away from the NH_2 group.

In conclusion, the structure of the first solvation shell in $An^+-(N_2)_n$ suggested in Figure 6 is clearly recognizable in the frequency shifts of both ν_{av} and $2\nu_b$ as a function of the cluster size (Figure 5). The first two N_2 ligands form equivalent H bonds to the amino group of An^+, leading to red shifts in ν_{av} and blue shifts in $2\nu_b$. After this first subshell is completed, the next two ligands form probably π bonds to the ipso C atom, leading to blue shifts in ν_{av} and red shifts in $2\nu_b$. Further ligands occupy less favorable ring binding sites with smaller effects on the vibrational properties of the amino group.

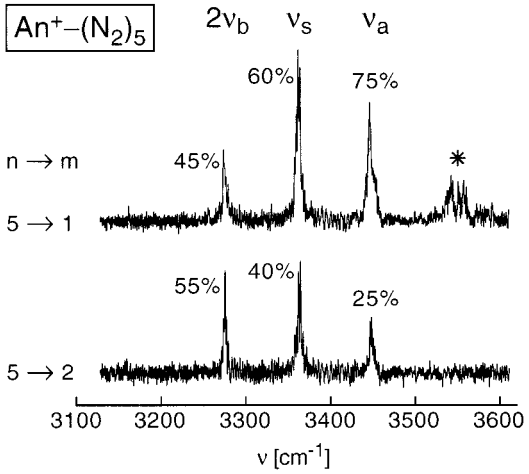

Figure 7. Comparison of the EI−IR photodissociation spectra of $An^+-(N_2)_5$ recorded simultaneously in the An^+-N_2 ($m = 1$) and $An^+-(N_2)_2$ ($m = 2$) fragment channels. The transition marked with an asterisk at $\nu \sim 3550$ cm^{-1} originates from the $H_5O_2^+-(N_2)_7$ contamination. The ratio of the integrated transition intensities observed in the $m = 1$ and $m = 2$ fragment channel (in %) are given for the ν_s, ν_a, and $2\nu_b$ resonances of $An^+-(N_2)_5$, respectively. The accuracy of these values is estimated as ±5%.

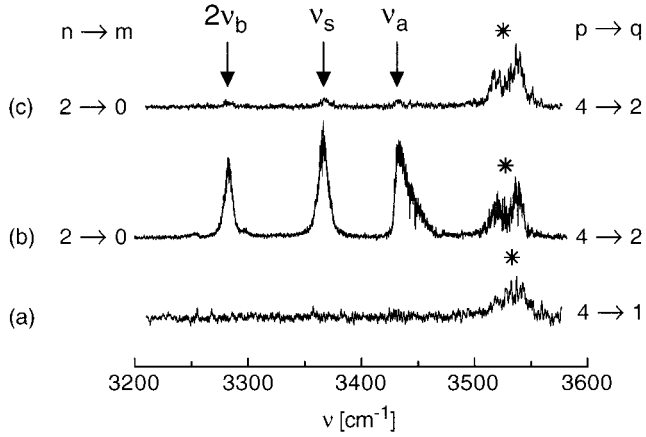

Figure 8. Comparison of EI−IR photodissociation spectra obtained for setting the first quadrupole at $m = 149$ u, corresponding to the mass of $An^+-(N_2)_2$ and $H_5O_2^+-(N_2)_4$. The spectrum in trace a is recorded for the second quadrupole set to $m = 65$ u, corresponding to the mass of $H_5O_2^+-N_2$. The spectra in traces b and c are recorded for the second quadrupole set to $m = 93$ u, corresponding to the mass of An^+ and $H_5O_2^+-(N_2)_2$. The spectra of traces b and c are obtained before and after (almost completely) removing An from the gas inlet system. Spectra a and b are recorded simultaneously. The transitions ν_a, ν_s, and $2\nu_b$ are assigned to $An^+-(N_2)_2$, whereas the transition marked with an asterisk is attributed to $H_5O_2^+-(N_2)_4$.

According to eq 2, several $An^+-(N_2)_m$ fragment channels may be observed for a given $An^+-(N_2)_n$ parent cluster with $n > 1$ (abbreviated as $n \rightarrow m$ in Figures 4, 7, and 8). The number of evaporated ligands depends sensitively on the cluster size, the excitation frequency, and the internal energy prior to photoexcitation. For example, Figure 7 shows the IR spectra of $An^+-(N_2)_5$ recorded in the $An^+-(N_2)_2$ and An^+-N_2 fragment channels, corresponding to the loss of 3 and 4 N_2 ligands upon vibrational excitation. Table 3 summarizes the fragmentation branching ratios measured for ν_s excitation of $An^+-(N_2)_n$. Similar to related A^+-L_n cluster systems studied previously

TABLE 3: Photofragmentation Branching Ratios (in %) of $An^+-(N_2)_n$ Complexes for the Photoinduced Reaction in Eq 2 Measured at the Band Maxima of the ν_s Transition[a]

n	$m = 0$	$m = 1$	$m = 2$
1,2	100		
3	90	10	
4	5	95	
5		60	40

[a] The accuracy of the values is estimated as ±5%.

with the same experimental approach,[23,35,42,44,46,49,50] the range of observed fragment channels is rather narrow. With the exception of the $n = 5$ complex, the action signal of all $An^+-(N_2)_n$ clusters investigated appears with more than 90% in a single fragment channel. This information can thus be used to derive approximate ligand binding energies, assuming a simple statistical model for the evaporation process. The basic assumptions of this model are outlined in refs 23 and 35. The model assumes that the energy of the absorbed photon is used for ligand evaporation (only single photon absorption processes are observed for the employed laser intensities of $<10^{-1}$ mJ/mm^2). Hence, the photon energy must be larger than the binding energy of the $n - m$ evaporated ligands but smaller than the sum of the dissociation energies of the $n - m + 1$ most weakly bound ligands. Moreover, ligands solvated at equivalent positions are assumed to have the same binding energy. For this purpose, the N_2 molecules in $An^+-(N_2)_n$ are classified into H-bound and π-bound ligands with dissociation energies of D_0(H) and $D_0(\pi)$, respectively. The analysis of the data in Table 3 leads to D_0(H) $\sim 1100 \pm 300$ cm^{-1} and $D_0(\pi) \sim 700 \pm 200$ cm^{-1}, in good agreement with D_e(H) = 1431 cm^{-1} and $D_e(\pi) = 742$ cm^{-1} calculated at the UMP2 level (Figure 2). The relative intensities of corresponding bands of $An^+-(N_2)_5$ appearing in the $m = 1$ and 2 fragment channels depend on the excitation frequency (Figure 7). In general, the larger the available internal energy after IR excitation, the higher the probability for the loss of more N_2 ligands. For example, the ratio of the integrated transition intensities in the $m = 1$ and 2 fragment channel increases from 45% for the $2\nu_b$ band at 3274 cm^{-1} to 75% for the ν_a band at 3447 cm^{-1}. In addition, the widths of the bands recorded in the $m = 2$ channel are slightly narrower than those in the $m = 1$ channel. This observation indicates that the parent complexes contributing to the $m = 1$ channel contain more internal energy prior to IR excitation than those contributing to the $m = 2$ channel and can thus evaporate more ligands after vibrational excitation. In contrast to the widths and relative intensities, the peak positions are nearly independent of the fragment channel.

In the following discussion, the carrier of the transitions marked by asterisks in Figures 4, 7, and 8 is identified as $H_5O_2^+-(N_2)_p$ contamination of the $An^+-(N_2)_n$ mass channel with $n = p + 2$. The observation of $H_5O_2^+$ (37 u) and $H_5O_2^+-N_2$ (65 u) in the mass spectrum of the ion source suggests that larger $H_5O_2^+-(N_2)_p$ clusters are also produced in the expansion (section 2). Thus, two processes have to be considered for the analysis of the $An^+-(N_2)_n$ IR action spectra:

$$An^+-(N_2)_n + \nu_{IR} \rightarrow An^+-(N_2)_m + (n-m)N_2 \quad (3a)$$

$$H_5O_2^+-(N_2)_p + \nu_{IR} \rightarrow H_5O_2^+-(N_2)_q + (p-q)N_2 \quad (3b)$$

The following arguments confirm that process 3b with $p = n + 2$ and $q = m + 2$ gives rise to the transitions marked by asterisks. The relative intensities of the ν_s, ν_a, and $2\nu_b$ transitions of $An^+-(N_2)_n$ and the "asterisk transitions" strongly depend on the An concentration in the expansion. This is demonstrated by the spectra in Figure 8 parts b and c for $n = 2$, which have been recorded before and after (almost completely) removing An from the gas inlet system. Comparison of both spectra clearly confirm that all transitions in Figure 4 assigned to $An^+-(N_2)_n$ are indeed originating from this cluster series, whereas the asterisk transitions have to be assigned to a different carrier. The contamination must be of the form $X^+-(N_2)_p$, as the corresponding CID (recorded by adding He as collision gas to the octopole) and LID signals are observed in fragment channels spaced by N_2 mass units ($\Delta m = 28$ u). Moreover, the CID spectra of ions with the mass 93 u show sequential loss of N_2 ligands down to mass 37 u ($H_5O_2^+$), indicating that both An^+ and $H_5O_2^+-(N_2)_2$ provide significant contributions to the signal in the 93 u mass channel. The presence of water ligands in the larger $H_5O_2^+-(N_2)_p$ impurity ions is confirmed by their CID spectra, showing the loss of H_2O according to $H_5O_2^+$ dissociation into H_3O^+ and H_2O. In addition, the O−H stretch vibrations of $H_5O_2^+-(N_2)_p$ clusters are expected in the spectral range between 3500 and 3700 cm^{-1}.[51] The appearance of $H_5O_2^+-(N_2)_p$ signals in the IR spectra of $An^+-(N_2)_n$ in Figure 4 requires not only the coincidence of the parent ion mass but also of the daughter ion mass; that is, the same number of N_2 ligands have to be evaporated upon vibrational excitation. This condition is only fulfilled for $n > 1$. The An^+-N_2 dimer spectrum is free from interference with the $H_5O_2^+-(N_2)_3$ contamination (Figure 4) because the first complex can only lose one N_2 ligand (a single photon with $\nu \sim 3400$ cm^{-1} cannot break covalent bonds in An^+), whereas the second complex evaporates two ligands. Comparison of parts a and b of Figure 8 shows that the transition(s) of $H_5O_2^+-(N_2)_4$ appear in both the $H_5O_2^+-N_2$ and $H_5O_2^+-(N_2)_2$ fragment channels (loss of 3 and 2 N_2 ligands), whereas the $An^+-(N_2)_2$ bands can only be seen in the An^+ fragment channel (loss of 2 ligands). All mentioned observations unambiguously identify $H_5O_2^+-(N_2)_p$ as the carrier of the asterisk bands. A detailed analysis of these transitions is, however, beyond the scope of the present work.

4.3. Further Discussion. Owing to the additional charge, the intermolecular PES of the An^+-N_2 cation is rather different from that of the neutral dimer. Hence, it is not surprising that both complexes have very different equilibrium geometries. Spectroscopy at the level of rotational resolution is compatible with a π-bound sandwich-like equilibrium geometry for neutral $An-N_2$ in both the S_0 and S_1 states,[20] with the N_2 ligand lying above the aromatic ring in a parallel configuration. Such a structure is favored by dispersion forces and the electrostatic quadrupole−quadrupole interaction. Calculations at the MP2/6-31G* level performed in the present work confirm that the π-bound structure is indeed the global minimum on the PES in the S_0 state, whereas the H-bound structure is less stable. In the cation ground state, significant additional contributions to the attractive part of the intermolecular potential arise from the electrostatic and induction forces of the charge distribution in An^+ interacting with the negative quadrupole moment and anisotropic polarizability of N_2. In general, the anisotropy of the latter long-range forces aligns the N_2 ligand in such a way that it points toward the positive charge.[4,22,43,52,53] The analysis of the charge distribution in An^+ reveals large positive partial charges on the ipso C atom and both protons of the NH_2 group.[11] Hence, the N_2 ligand is roughly directed to the ipso C atom in π-bound An^+-N_2 and forms a nearly linear proton bond in H-bound An^+-N_2 (Figure 2). Contrary to neutral $An-N_2$, the H-bound structure of An^+-N_2 is far more stable than the π-bound isomer.

The ionization-induced structural effects observed for $An-N_2$ are similar to those of the related An−Ar complex.[11] Neutral An−Ar has a π-bound global minimum in the S_0 state,[6−8] whereas H-bound An−Ar is calculated to be a less stable local minimum.[11] On the other hand, the global minimum of An^+-Ar corresponds to the H-bound structure, whereas the π-bound geometry is a less stable local minimum.[11,12] The intermolecular bonds in H-bound and π-bound An^+-Ar[11] are, however, significantly longer and weaker than in An^+-N_2, mainly owing to the additional charge−quadrupole attraction present in the latter complex.[23] For example, the dissociation energies calculated at the UMP2/6-311G(2df,2pd) level are $D_e(\pi) = 454$ and 742 cm^{-1} and $D_e(H) = 513$ and 1431 cm^{-1} for An^+-Ar and An^+-N_2, respectively. The stronger intermolecular bonds in An^+-N_2 lead to larger vibrational frequency shifts. For example, $\Delta\nu_s = -21$ and $\Delta\nu_a = -18$ cm^{-1} for H-bound An^+-N_2 and $\Delta\nu_s = -12$ and $\Delta\nu_a = -9$ cm^{-1} for H-bound An^+-Ar. In line with the stronger intermolecular proton bonds, the retarding force for the intramolecular bending motion of the NH_2 group is also larger for complexation with N_2 than with Ar. Consequently, the $2\nu_b$ overtone of H-bound An^+-N_2 is 7 cm^{-1} blue shifted compared to the same vibration in H-bound An^+-Ar.

The large structural changes upon ionization of $An-N_2$ have important implications for the interpretation of its photoionization spectra, including the ZEKE and REMPI−IR spectra of An^+-N_2. The large differences in the global minima of $An-N_2$ in $S_{0,1}$ and D_0 imply that the global H-bound An^+-N_2 minimum is not directly accessed by vertical (REMPI) ionization of neutral π-bound $An-N_2$ because of vanishing FC factors. Consequently, the ZEKE spectra of π-bound $An-N_2$ reported in refs 19 and 21 correspond almost certainly to ionization into the π-bound An^+-N_2 cation. However, as the position and orientation of the N_2 ligand is rather different in π-bound $An-N_2$ and An^+-N_2, the transitions observed in the ZEKE spectra correspond to significant excitation of low-frequency intermolecular modes (including stretching, bending, and internal rotation motions). Moreover, the origin transition between π-bound $An-N_2$ (S_1) and π-bound An^+-N_2 (D_0) has probably been missed in the ZEKE spectra, and the conclusions about the dissociation energy of π-bound An^+-N_2 derived from the assignment of a wrong adiabatic ionization energy (AIE) are not reliable.[19] For example, the upper limit of the dissociation energy of the π-bound An^+-N_2 is derived as 470 cm^{-1} from the dissociation energy of π-bound $An-N_2$ in the S_0 state (<420 cm^{-1})[17] and the incorrect AIE (shift <50 cm^{-1}) determined in ref 19. This dissociation energy is significantly lower than the more reliable value of 700 ± 200 cm^{-1} determined in the present work. As the H-bound isomer of An^+-N_2 is much lower in energy than the π-bound isomer, the adiabatic IE determined by ZEKE spectroscopy of π-bound $An-N_2$ is clearly not the true AIE of this dimer (as stated in ref 19). Similar incorrect determinations of AIE values derived from photoionization spectra have previously been reported for related systems, such as Ph−Ar and An−Ar.[11,23]

Interestingly, the REMPI−IR spectrum of An^+-N_2 obtained by (1+1) REMPI of π-bound $An-N_2$ (excess energy of ~5000 cm^{-1}) shows the signature of H-bound An^+-N_2 (Figure 3b). This observation indicates that isomerization can occur after ionization on the time scale of 50 ns (the delay between the ionization and IR laser pulses).[18] The ZEKE spectra of π-bound An^+-N_2 show regular vibrational structure in the intermolecular bending vibration along the isomerization coordinate,[19] suggesting that the barrier to isomerization from the π-bound local minimum toward the H-bound global minimum of An^+-N_2 is substantial. Hence, to overcome the isomerization barrier the excitation of intramolcular vibrations of π-bound An^+-N_2 above this barrier is required in the (1+1) REMPI process. Moreover, these vibrations have to be either below the lowest dissociation threshold of An^+-N_2 or, if this is not the case, predissociation from these levels has to be slower than 50 ns. In both cases, ionization of π-bound $An-N_2$ is followed by isomerization to produce vibrationally excited H-bound An^+-N_2 dimers, which contribute to the REMPI−IR spectrum in Figure 3b. In contrast to the REMPI−IR spectrum of An^+-N_2, the corresponding REMPI−IR spectrum of the related An^+-Ar complex does not reveal transitions of the global H-bound minimum.[27] Thus, the isomerization process after (1+1) REMPI does not occur for π-bound An^+-Ar, either because of its lower dissociation energy or shorter predissociation lifetimes of its intramolecular vibrations.[11]

The strength of the intermolecular interaction in proton-bound complexes AH^+-N_2 is related to the proton affinity (PA) of the base A.[4] The smaller PA(A), the stronger and shorter the intermolecular bond. For example, as C_6H_5NH and c-C_3H_2 have similar PAs (950 and 934 kJ/mol),[54] the intermolecular bonds in H-bound An^+-N_2 and c-$C_3H_3-N_2$ have similar dissociation energies and intermolecular H−N separations:[55] the values calculated at the MP2/6-311G(2df,2pd) level are $D_e = 1431$ and 1227 cm^{-1} and $R_e = 2.17$ and 2.18 Å, respectively. On the other hand, stronger intermolecular AH^+-N_2 bonds are observed for bases A with smaller PAs, such as SiO and C_6H_5O.[22,43] In line with PA(Ar) < PA(N_2), the interaction in H-bound An^+-Ar is weaker than in H-bound An^+-N_2.

It is interesting to compare the structures and interaction strengths of the isoelectronic $An-N_2$ and $Ph-N_2$ complexes and their cations. In contrast to π-bound $An-N_2$, $Ph-N_2$ prefers the H-bound over the π-bound structure in the neutral S_0 state,[31,33] because the dipole−quadrupole interaction (favoring the H-bound structure) overrides the dispersion and quadrupole−quadrupole interactions (favoring the π-bound structure). On the other hand, the additional charge−quadrupole interaction clearly favors H-bound equilibrium structures for both cation complexes.[22,23,31,33] In general, the microsolvation of An^+ and Ph^+ in molecular N_2 is very similar. The first N_2 ligand(s) form nearly linear H bond(s) to the NH_2/OH group of An^+/Ph^+, and further ligands bind to the aromatic ring. In line with PA(C_6H_5O) < PA(C_6H_5NH),[54,56] the measured dissociation energy of the H bond in Ph^+-N_2 is larger than in An^+-N_2: $D_0(H) = 1640 \pm 10$ and 1100 ± 300 cm^{-1}, respectively.[57] On the other hand, the π bonds feature similar binding energies for both aromatic ions: $D_0(\pi) = 750 \pm 150$ and 700 ± 200 cm^{-1}, respectively.[23]

5. Concluding Remarks

The intermolecular interaction between the An^+ cation and inert N_2 ligands is investigated by means of EI−IR spectroscopy and quantum chemical calculations of $An^+-(N_2)_n$ clusters with $n \leq 5$. Both the IR spectrum and the calculations agree that the global minimum on the PES of the An^+-N_2 dimer corresponds to a H-bound structure, in which the N_2 ligand forms a (nearly) linear H bond to one proton of the amino group of An^+. The π-bound An^+-N_2 structure, in which the N_2 molecule binds in a perpendicular fashion to the ipso C atom of An^+, is calculated to be a local minimum on the PES. This isomer is not detected in the EI−IR spectrum of the dimer. In general, the structures of the H-bound and π-bound An^+-N_2 cations are rather different from the neutral π-bound $An-N_2$ global minimum structure, demonstrating the drastic effects of ionization on the

shape of the PES. The photofragmentation branching ratios and systematic vibrational frequency shifts in the IR spectra of $An^+-(N_2)_n$ provide information about the microsolvation process of An^+ in a quadrupolar polarizable solvent. The first two N_2 ligands fill a first subshell by solvating the protons of the amino group (H bonds), and further ligands bind to the aromatic ring (π bonds). The dissociation energies of the H and π bonds are estimated from the photofragmentation data as $D_0(H) \sim 1100 \pm 300$ cm^{-1} and $D_0(\pi) \sim 700 \pm 200$ cm^{-1}, respectively. These values are in good agreement with the corresponding well depths of $D_e(H) = 1431$ cm^{-1} and $D_0(\pi) = 742$ cm^{-1} calculated at the UMP2/6-311G(2df,2pd) level. In general, the $An^+-(N_2)_n$ microsolvation process is found to be similar to those observed for An^+-Ar_n and isoelectronic $Ph^+-(N_2)_n$.

Acknowledgment. This study is part of Project No. 20-63459.00 of the Swiss National Science Foundation. O.D. is supported by the Deutsche Forschungsgemeinschaft via a Heisenberg Fellowship (DO 729/1-1). We thank A. Fujii for providing the vibrational frequencies of the aniline cation prior to publication.

References and Notes

(1) March, J. *Advanced Organic Chemistry: Reactions, Mechanisms, and Structure*; Wiley: New York, 1985.
(2) Hobza, P.; Zaharadnik, R. *Intermolecular complexes: The Role of van der Waals Systems in Physical Chemistry and in the Biodisciplines*; Elsevier: Amsterdam, 1988.
(3) Jeffrey, G. A.; Saenger, W. *Hydrogen bonding in biological systems*; Springer: Heidelberg, Germany, 1991.
(4) Bieske, E. J.; Dopfer, O. *Chem. Rev.* **2000**, *100*, 3963.
(5) Stryer, L. *Biochemistry*; Freeman: New York, 1996.
(6) Sinclair, W. E.; Pratt, D. W. *J. Chem. Phys.* **1996**, *105*, 7942.
(7) Becucci, M.; Pietraperzia, G.; Lakin, N. M.; Castellucci, E.; Bréchignac, P. *Chem. Phys. Lett.* **1996**, *260*, 87.
(8) Storm, V.; Dreizler, H.; Consalvo, D. *Chem. Phys.* **1998**, *237*, 395.
(9) Consalvo, D.; Storm, V.; Dreizler, H. *Chem. Phys.* **1998**, *228*, 301.
(10) Yamanouchi, K.; Isogai, S.; Tsuchiya, S.; Kuchitsu, K. *Chem. Phys.* **1987**, *116*, 123.
(11) Solcà, N.; Dopfer, O. *Eur. Phys. J. D* **2002**. In press.
(12) Nakanaga, T.; Ito, F. *Chem. Phys. Lett.* **2002**, *355*, 109.
(13) Spoerel, U.; Stahl, W. *J. Mol. Spectrosc.* **1998**, *190*, 278.
(14) Nakanaga, T.; Kawamata, K.; Ito, F. *Chem. Phys. Lett.* **1997**, *279*, 309.
(15) Nakanaga, T.; Ito, F. *Chem. Phys. Lett.* **2001**, *348*, 270.
(16) Yamanouchi, K.; Isogai, S.; Tsuchiya, S. *J. Mol. Struct.* **1986**, *146*, 349.
(17) Hineman, M. F.; Kim, S. K.; Bernstein, E. R.; Kelley, D. F. *J. Chem. Phys.* **1992**, *96*, 4904.
(18) Schmid, R. P.; Chowdhury, P. K.; Miyawaki, J.; Ito, F.; Suguwara, K.; Nakanaga, T.; Takeo, H.; Jones, H. *Chem. Phys.* **1997**, *218*, 291.
(19) Jäckel, J. G.; Jones, H. *Chem. Phys.* **1999**, *247*, 321.
(20) Schäfer, M.; Pratt, D. W. *J. Chem. Phys.* **2001**, *115*, 11147.
(21) Smith, J. M.; Zhang, X.; Knee, J. L. *J. Chem. Phys.* **1993**, *99*, 2550.
(22) Solcà, N.; Dopfer, O. *Chem. Phys. Lett.* **2000**, *325*, 354.
(23) Solcà, N.; Dopfer, O. *J. Phys. Chem. A* **2001**, *105*, 5637.
(24) Takahashi, M.; Ozeki, H.; Kimura, K. *J. Chem. Phys.* **1992**, *96*, 6399.
(25) Zhang, X.; Smith, J. M.; Knee, J. L. *J. Chem. Phys.* **1992**, *97*, 2843.
(26) Piest, H.; von Helden, G.; Meijer, G. *J. Chem. Phys.* **1999**, *110*, 2010.
(27) Nakanaga, T.; Ito, F.; Miyawaki, J.; Sugawara, K.; Takeo, H. *Chem. Phys. Lett.* **1996**, *261*, 414.
(28) Fujii, A.; Sawamura, T.; Tanabe, S.; Ebata, T.; Mikami, N. *Chem. Phys. Lett.* **1994**, *225*, 104.
(29) Zhang, X.; Knee, J. L. *Faraday Discuss.* **1994**, *97*, 299.
(30) Dessent, C. E. H.; Haines, S. R.; Müller-Dethlefs, K. *Chem. Phys. Lett.* **1999**, *315*, 103.
(31) Fujii, A.; Miyazaki, M.; Ebata, T.; Mikami, N. *J. Chem. Phys.* **1999**, *110*, 11125.
(32) Solcà, N.; Dopfer, O. *J. Mol. Struct.* **2001**, *563−564*, 241.
(33) Haines, S. R.; Geppert, W. D.; Chapman, D. M.; Watkins, M. J.; Dessent, C. E. H.; Cockett, M. C. R.; Müller-Dethlefs, K. *J. Chem. Phys.* **1998**, *109*, 9244.
(34) Solcà, N.; Dopfer, O. *Chem. Phys. Lett.* **2001**, *347*, 59.
(35) Nizkorodov, S. A.; Dopfer, O.; Ruchti, T.; Meuwly, M.; Maier, J. P.; Bieske, E. J. *J. Phys. Chem.* **1995**, *99*, 17118.
(36) Linstrom, P. J.; Mallard, W. G. *NIST Chemistry WebBook, NIST Standard Reference Database Number 69*, 2001 (http://webbook.nist.gov).
(37) Guelachvili, G.; Rao, K. N. *Handbook of Infrared Standards*; Academic Press: London, 1993.
(38) Frisch, M. J.; Trucks, G. W.; Schlegel, H. B.; Scuseria, G. E.; Robb, M. A.; Cheeseman, J. R.; Zakrzewski, V. G.; Montgomery, J. A., Jr.; Stratmann, R. E.; Burant, J. C.; Dapprich, S.; Millam, J. M.; Daniels, A. D.; Kudin, K. N.; Strain, M. C.; Farkas, O.; Tomasi, J.; Barone, V.; Cossi, M.; Cammi, R.; Mennucci, B.; Pomelli, C.; Adamo, C.; Clifford, S.; Ochterski, J.; Petersson, G. A.; Ayala, P. Y.; Cui, Q.; Morokuma, K.; Malick, D. K.; Rabuck, A. D.; Raghavachari, K.; Foresman, J. B.; Cioslowski, J.; Ortiz, J. V.; Stefanov, B. B.; Liu, G.; Liashenko, A.; Piskorz, P.; Komaromi, I.; Gomperts, R.; Martin, R. L.; Fox, D. J.; Keith, T.; Al-Laham, M. A.; Peng, C. Y.; Nanayakkara, A.; Gonzalez, C.; Challacombe, M.; Gill, P. M. W.; Johnson, B. G.; Chen, W.; Wong, M. W.; Andres, J. L.; Head-Gordon, M.; Replogle, E. S.; Pople, J. A. *Gaussian 98*, revision A.5; Gaussian, Inc.: Pittsburgh, PA, 1998.
(39) Boys, S. F.; Bernardi, F. *Mol. Phys.* **1970**, *19*, 553.
(40) Fujii, A. Private communication, 2001.
(41) Gée, C.; Douin, S.; Crépin, C.; Bréchignac, P. *Chem. Phys. Lett.* **2001**, *338*, 130.
(42) Dopfer, O.; Roth, D.; Maier, J. P. *J. Phys. Chem. A* **2000**, *104*, 11702.
(43) Olkhov, R. V.; Dopfer, O. *Chem. Phys. Lett.* **1999**, *314*, 215.
(44) Olkhov, R. V.; Nizkorodov, S. A.; Dopfer, O. *Chem. Phys.* **1998**, *239*, 393.
(45) Dopfer, O.; Solcà, N.; Olkhov, R. V.; Maier, J. P. *Chem. Phys.* In press.
(46) Olkhov, R. V.; Nizkorodov, S. A.; Dopfer, O. *J. Chem. Phys.* **1998**, *108*, 10046.
(47) Dopfer, O. *J. Phys. Chem. A* **2000**, *104*, 11693.
(48) Dopfer, O. *Chem. Phys.* In press.
(49) Dopfer, O.; Roth, D.; Maier, J. P. *Int. J. Mass. Spectrom.* In press.
(50) Dopfer, O.; Nizkorodov, S. A.; Meuwly, M.; Bieske, E. J.; Maier, J. P. *Int. J. Mass. Spectrom. and Ion Proc.* **1997**, *167/168*, 637.
(51) Yeh, L. I.; Okumura, M.; Myers, J. D.; Price, J. M.; Lee, Y. T. *J. Chem. Phys.* **1989**, *91*, 7319.
(52) Robbins, D. L.; Brock, L. R.; Pilgrim, J. S.; Duncan, M. A. *J. Chem. Phys.* **1995**, *102*, 1481.
(53) Pullins, S. H.; Reddic, J. E.; France, M. R.; Duncan, M. A. *J. Chem. Phys.* **1998**, *108*, 2725.
(54) Hunter, E. P.; Lias, S. G. J. *J. Phys. Chem. Ref. Data* **1998**, *27*, 413.
(55) Dopfer, O.; Roth, D.; Maier, J. P. *J. Am. Chem. Soc.* **2002**, *124*, 494.
(56) Kim, H. T.; Green, R. J.; Qian, J.; Anderson, S. L. *J. Chem. Phys.* **2000**, *112*, 5717.
(57) Haines, S. R.; Dessent, C. E. H.; Müller-Dethlefs, K. *J. Chem. Phys.* **1999**, *111*, 1947.